Article

Structure

Crystal Structure of the 3.8-MDa Respiratory Supermolecule Hemocyanin at 3.0 Å Resolution

Graphical Abstract

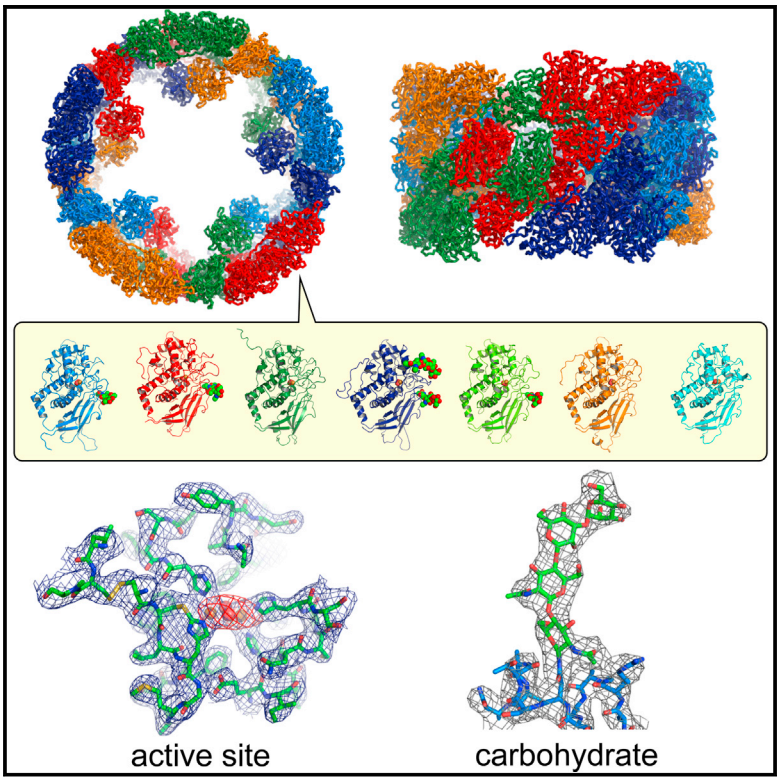

Authors

Zuoqi Gai, Asuka Matsuno, Koji Kato, ..., Tohru Terada, Yoshikazu Tanaka, Min Yao

Correspondence

tanaka@sci.hokudai.ac.jp

In Brief

Gai et al. determined the first X-ray crystal structure of intact molluscan hemocyanin, which unveiled the architecture of the 3.8-MDa cylindrical supermolecule composed of hierarchically associated homologous functional units. Roles of the inner collar domains and carbohydrates, and evolutionary implications, are discussed in detail.

Highlights

- First crystal structure of intact molluscan hemocyanin was determined
- The entire hemocyanin is composed of FU dimer building blocks
- Rigid FU dimers formed by specific interactions assemble with flexibility
- Roles of the carbohydrates and evolutionary implications are revealed

Accession Numbers

4YD9
AB897790

Gai et al., 2015, Structure *23*, 2204–2212
December 1, 2015
http://dx.doi.org/10.1016/j.str.2015.09.008

CellPress

Structure
Article

Crystal Structure of the 3.8-MDa Respiratory Supermolecule Hemocyanin at 3.0 Å Resolution

Zuoqi Gai,[1,7] Asuka Matsuno,[2,7] Koji Kato,[1,2,7] Sanae Kato,[3] Md Rafiqul Islam Khan,[3] Takeshi Shimizu,[4] Takeya Yoshioka,[4] Yuki Kato,[4] Hideki Kishimura,[5] Gaku Kanno,[5] Yoshikatsu Miyabe,[5] Tohru Terada,[6] Yoshikazu Tanaka,[1,2,*] and Min Yao[1,2]

[1]Laboratory of X-Ray Structural Biology, Faculty of Advanced Life Science, Hokkaido University, Sapporo 060-0810, Japan
[2]Laboratory of X-Ray Structural Biology, Graduate School of Life Science, Hokkaido University, Sapporo 060-0810, Japan
[3]Department of Biochemistry, Asahikawa Medical University, Asahikawa 078-8510, Japan
[4]Food Science Division, Hokkaido Industrial Technology Center, Hakodate 041-0801, Japan
[5]Division of Marine Life Science, Graduate School of Fisheries Science, Hokkaido University, Hakodate 041-8611, Japan
[6]Agricultural Bioinformatics Research Unit, Graduate School of Agricultural and Life Sciences, The University of Tokyo, Tokyo 113-8657, Japan
[7]Co-first author
*Correspondence: tanaka@sci.hokudai.ac.jp
http://dx.doi.org/10.1016/j.str.2015.09.008

SUMMARY

Molluscan hemocyanin, a copper-containing oxygen transporter, is one of the largest known proteins. Although molluscan hemocyanins are currently applied as immunotherapeutic agents, their precise structure has not been determined because of their enormous size. Here, we have determined the first X-ray crystal structure of intact molluscan hemocyanin. The structure unveiled the architecture of the 3.8-MDa supermolecule composed of homologous functional units (FUs), wherein the dimers of FUs hierarchically associated to form the entire cylindrical decamer. Most of the specific inter-FU interactions were localized at narrow regions in the FU dimers, suggesting that rigid FU dimers formed by specific interactions assemble with flexibility. Furthermore, the roles of carbohydrates in assembly and allosteric effect, and conserved sulfur-containing residues in copper incorporation, were revealed. The precise structural information obtained in this study will accelerate our understanding of the molecular basis of hemocyanin and its future applications.

INTRODUCTION

Many molluscs and arthropods are characterized by the presence of blue blood because their oxygen transporter, hemocyanin, is a type-3 copper-containing protein. Hemocyanin is a large multimeric glycoprotein, freely dissolved in the hemolymph. Molluscan hemocyanin is a decamer (cephalopods) or multidecamer (gastropods) with subunits of approximately 330–450 kDa, which result in a total molecular mass larger than 3.3 MDa (Markl, 2013). Therefore, molluscan hemocyanin is one of the largest known proteins. The molluscan hemocyanin polypeptide is composed of a subset of sequentially arranged paralogous functional units (FUs) of approximately 50 kDa. Ten copies of the polypeptide assemble into a cylinder of 310 Å in diameter and 160 Å in height. In gastropods, several cylindrical decamers further stack into di- or multidecamers (Markl, 2013).

Since its discovery in 1879, the biochemical and biophysical characteristics of hemocyanin have been extensively investigated. Molluscan hemocyanins are currently applied as adjuvants for antibody preparation (Becker et al., 2014). Notably, molluscan hemocyanin is further acknowledged as an immunotherapeutic agent in the treatment of cancer and as a carrier molecule for vaccines (Becker et al., 2014). These valuable properties are a result of the vast size of hemocyanin as well as the presence of attached glycans (Geyer et al., 2005; Harris and Markl, 1999; Siddiqui et al., 2007). To further explore its molecular basis and design effective hemocyanins for biomedical and biotechnological applications, precise structural information has been desired for a long time. However, its enormous size and propensity for dissociation have hampered crystal structure analysis of intact molluscan hemocyanin. Thus, structural studies of hemocyanin have mostly relied on electron microscopy (Boisset and Mouche, 2000; Gatsogiannis et al., 2007, 2015; Gatsogiannis and Markl, 2009; Lamy et al., 1998; Meissner et al., 2000; Zhang et al., 2013; Zhu et al., 2014), with crystal structure analysis being applied only to several FUs (Cuff et al., 1998; Jaenicke et al., 2010, 2011; Perbandt et al., 2003). Electron microscopy has indicated that the structure of molluscan hemocyanin is a hollow cylindrical wall with several collar regions located inside the cylinder (Gatsogiannis et al., 2007, 2015; Gatsogiannis and Markl, 2009; Zhang et al., 2013; Zhu et al., 2014). Although the architecture of FUs has been discussed on the basis of the cryoelectron microscopic structures, there is a limit to their validity for elucidation of detailed molecular mechanisms and/or for application to biomedical development owing to their low resolution; that is, for the intact form only a Cα model with no side chains is currently available (Zhang et al., 2013).

Most molluscan hemocyanins are composed of eight FUs (FU-a, -b, -c, -d, -e, -f, -g, and -h), whereas some cephalopod hemocyanins, such as those of octopuses and nautiluses, possess seven FUs (FU-a, -b, -c, -d, -e, -f, and -g), in which FU-h is lost. Hemocyanins from ten-armed cephalopods, such as cuttlefishes and squid, have an additional FU between FU-d

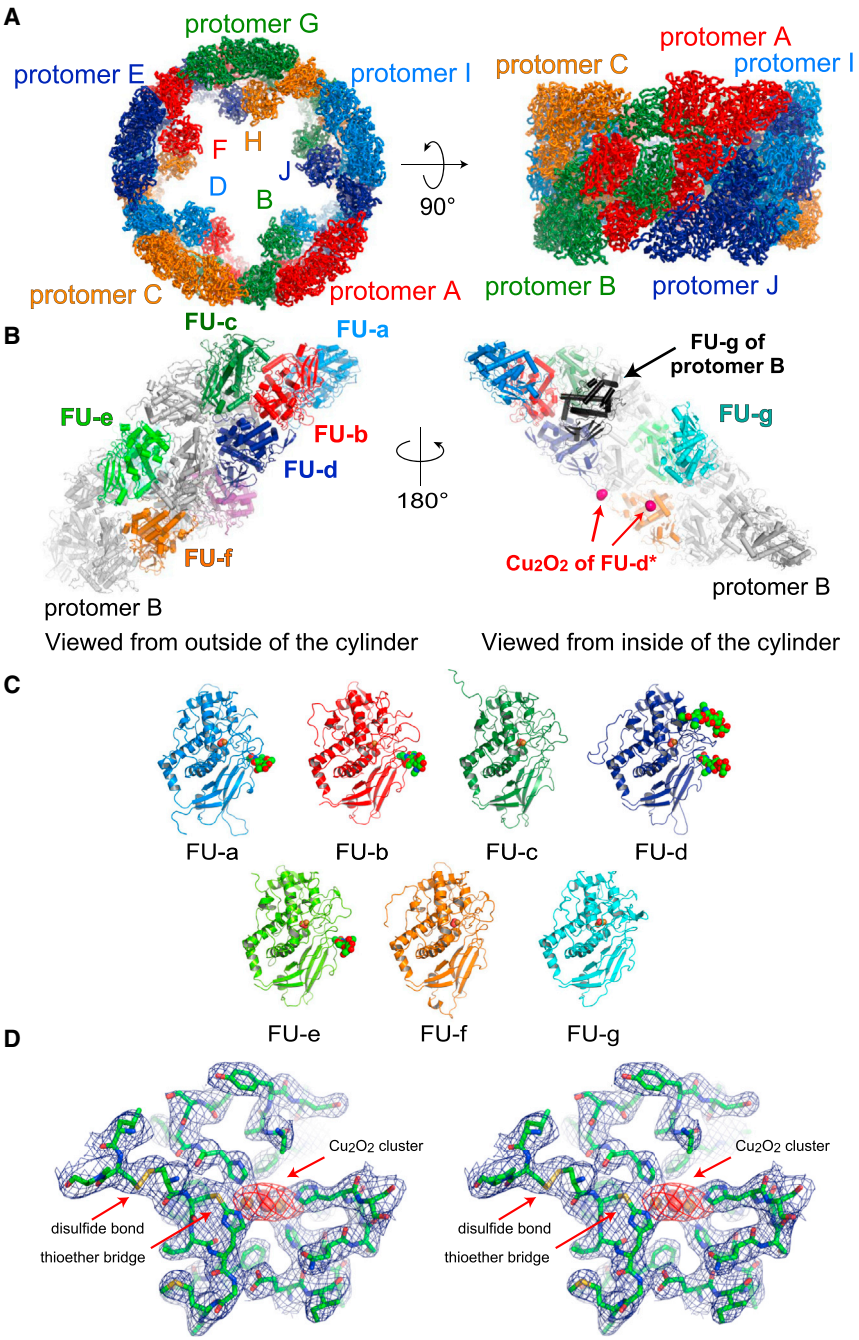

Figure 1. Crystal Structure of Hemocyanin

(A) Overall structure of intact decameric hemocyanin.

(B) Structure of a protomer colored according to functional units (FUs). For clarity, protomer B is also shown as gray. Cu_2O_2 clusters of FU-d* are shown as pink balls.

(C) Ribbon diagrams of all FUs. Colors correspond to (B). Carbohydrates and the Cu_2O_2 cluster are shown as spheres.

(D) Electron density around the Cu_2O_2 cluster (stereo representation). The $2F_o$-F_c map contoured at 1σ and the anomalous difference Fourier map derived from copper atoms contoured at 7.5σ are shown as dark blue and red, respectively. Cu and O atoms are shown as orange and red spheres, respectively.

See also Figures S1–S3 and Tables S1, S2, S3, and S4.

and -e (Thonig et al., 2014). Because of the significant sequence similarity with FU-d, this additional FU is designated as FU-d*, which yields the subunit structure of FU-a, -b, -c, -d, -d*, -e, -f, and -g (Markl, 2013; Thonig et al., 2014). Previous cryoelectron microscopic structures have shown that the cylindrical wall consists of FU-a–f, regardless of the FU composition, and remaining FUs assemble to form the inner collar regions (Gatsogiannis et al., 2007, 2015; Gatsogiannis and Markl, 2009; Zhang et al., 2013; Zhu et al., 2014).

In the present study, we successfully determined the X-ray crystal structure of the intact 3.8-MDa *Todarodes pacificus* (known as the Japanese flying squid, one of the typical squids of decapodiformes of cephalopods) hemocyanin at 3.0 Å resolution. On the basis of this first description of the atomic resolution structure, the molecular architecture of intact hemocyanin, roles of the inner collar domains and carbohydrates, and evolutionary implications are discussed in detail.

RESULTS AND DISCUSSION

Overall Crystal Structure of *T. pacificus* Hemocyanin

The crystal structure of *T. pacificus* hemocyanin was determined by the molecular replacement method using the wall region of the Cα model of *Haliotis diversicolor* hemocyanin (PDB: 3J32) as a search model combined with noncrystallographic symmetry (NCS) averaging (Figures 1 and S1, and Table 1). The revealed structure was a cylindrical decamer with five-fold symmetry, and consisted of a wall and five inner collars. The structure, finally refined at 3.0 Å resolution, consisted of 28,470 residues, 80 Cu_2O_2 clusters, and 50 carbohydrate moieties. This is the first description of the atomic structure of the entire molluscan hemocyanin. This atomic structure enables us to discuss the hemocyanin structure based purely on the experimental structure, which provides remarkably more precise information particularly in the wall region (see below), in contrast to the previous homology model structures.

Preceding the crystal structure analysis, we determined the amino acid sequence of *T. pacificus* hemocyanin. The hemocyanin subunit was composed of eight FUs, which share 39%–69% sequence identity (Figure S2 and Table S1). As previously observed for hemocyanin of cuttlefishes (Thonig et al., 2014), the fourth and fifth FUs show high sequence identity (69%). Hereafter, FUs are designated as FU-a, -b, -c, -d, -d*, -e, -f, and -g.

Table 1. Data Collection and Refinement Statistics

	Native	Cu Absorption Edge
Data Collection		
Space group	$P2_1$	$P2_1$
Cell dimensions		
a, *b*, *c* (Å)	171.4, 538.7, 310.9	171.9, 539.6, 312.5
α, β, γ (°)	90, 104.1, 90	90, 104.0, 90
Resolution (Å)[a]	13.42–3.00 (3.08–3.00)	49.41–5.15 (5.46–5.15)
R_{sym} (%)[a]	11.3 (75.1)	7.2 (16.0)
$<I/\sigma(I)>$[a]	7.76 (1.58)	10.37 (5.52)
Completeness (%)[a]	98.9 (99.3)	97.5 (97.2)
Redundancy[a]	2.56 (2.58)	1.97 (1.97)
Refinement		
Resolution (Å)	39.8–3.00	
No. of unique reflections	1,072,209	
R_{work}/R_{free}	0.2739/0.3031	
No. of atoms		
Protein	229,780	
Ligand/ion	2,050	
B factors (Å^2)		
Protein	76.7	
Ligand/ion	94.0	
RMSDs		
Bond lengths (Å)	0.011	
Bond angles (°)	1.402	

[a]Values in parentheses refer to data in the highest-resolution shell.

In the wall region, FU-a, -b, -c, -d, -e, and -f were unambiguously constructed based on the clear electron density. FU-a-b-c-d and FU-e-f, including linkers between FUs, were traced as continuous polypeptide chains (Figure S1D). The inner collars were composed of FU-d* and -g. The anomalous difference Fourier map of copper atoms and the NCS averaged electron density identified ten copies of FU-g sites located in the upper area of the cylinder lumen (Figures 1B and 2). FU-g occupies the same position as the FU-g dimer of the previously reported cryoelectron microscopic structures of other hemocyanins (Gatsogiannis and Markl, 2009; Gatsogiannis et al., 2007; Zhang et al., 2013). The electron density of FU-d* was observed in the bottom area of FU-g. Although the anomalous difference Fourier map clearly indicated the sites of copper, the NCS averaged electron density of FU-d* was intricately overlapped and was not adequately interpretable. Consequently, we could not construct the structure of FU-d*. Instead, we located only a Cu_2O_2 cluster on the copper sites of FU-d*. FU-d* should be located around this Cu_2O_2 cluster, although the precise orientation is unclear.

Although the FUs of the wall region were traced as two polypeptide fragments, i.e., fragments FU-a-b-c-d and FU-e-f, electron density connecting between the wall and the inner collar regions was invisible. Therefore, based solely on the electron density we were unable to connect all FUs into a single chain. A similar issue occurred also in cryoelectron microscopy analysis, i.e., two different pathways have been proposed (Gatsogiannis and Markl, 2009; Gatsogiannis et al., 2007; Zhang et al., 2013). Although both pathways are applicable for our crystal structure, to describe the assembly of protomers we expediently adopted that of *H. diversicolor* hemocyanin, determined based on the clear map of the linker regions (Figure 1A) (Zhang et al., 2013). Here, we discuss this structure as one of the possible models of the entire molluscan hemocyanin.

Each protomer forms a contact with five other protomers (Figure 1A and Table S1). For instance, protomer A interacts with protomers B, J, C, I, and D. Protomer A is related to protomers B and J by two different pseudo-two-fold axes perpendicular to the five-fold axis (note that this symmetry is applied only for the wall regions and not for the collar FUs), in which these protomers form contact mainly through the wall region. Protomers C and I are located on either side of protomer A with five-fold symmetry, whereas only a few contact regions are present here. Protomer D, located behind protomers B and C, forms an interaction with protomer A through the collar region. All ten protomers interact with five surrounding protomers in a similar manner, creating the hollow cylindrical hemocyanin composed of a wall with D_5 symmetry and symmetrically broken collars.

The buried surface area and hydrogen bonds between protomers A and B (and their equivalent contacts) is markedly larger than others (Table S1), indicating the significance of this interprotomer interaction in the decameric assembly. Previous studies revealed that dissociated hemocyanin has a warped plate-like structure (Harris et al., 2004; Miller et al., 1990), which likely corresponds to an A-B dimer. The plate-like dimers are arranged five-fold symmetrically, in which the adjacent two dimers assemble through the inner collar regions in addition to the contacts through the wall region. The collar is likely to reinforce the interaction between plate-like dimers by forming contact between protomers. Considering these observations together, it was concluded that the A-B dimer acts as a structural unit, which then assembles into a decamer with the help of the interaction through the collar domains.

It should be noted that two different orientations of the hemocyanin decamer intermingled in the crystal. As a consequence, the observed electron density showed D_5 symmetry regardless of the asymmetric arrangement of the inner collar region (Figure S1E). The inner collar region did not participate in the crystal packing, indicating that the orientation of the inner collar cannot influence the direction of decamer in the crystal. By means of X-ray crystallography, we observe the averaged electron density of all molecules in the crystal. In this case, intermingled packing of two vertically opposite decamers caused the pseudo-D_5 symmetry (Figure S3).

Architecture of the Decamer

All FUs have a quite similar structure regardless of their location on the wall or collar region (Figure 1C). The FUs were superposed on one another with root-mean-square deviation (RMSD) of <1.9 Å (Table S2). These observations indicate that this huge hollow cylindrical hemocyanin is built by assembling rather similar structural blocks.

All six FUs of the wall region formed similar dimeric assemblies, i.e., FU-(a-b), FU-(d-e), and FU-(c-f), in which the two FUs had pseudo-two-fold symmetry. These FU dimers were

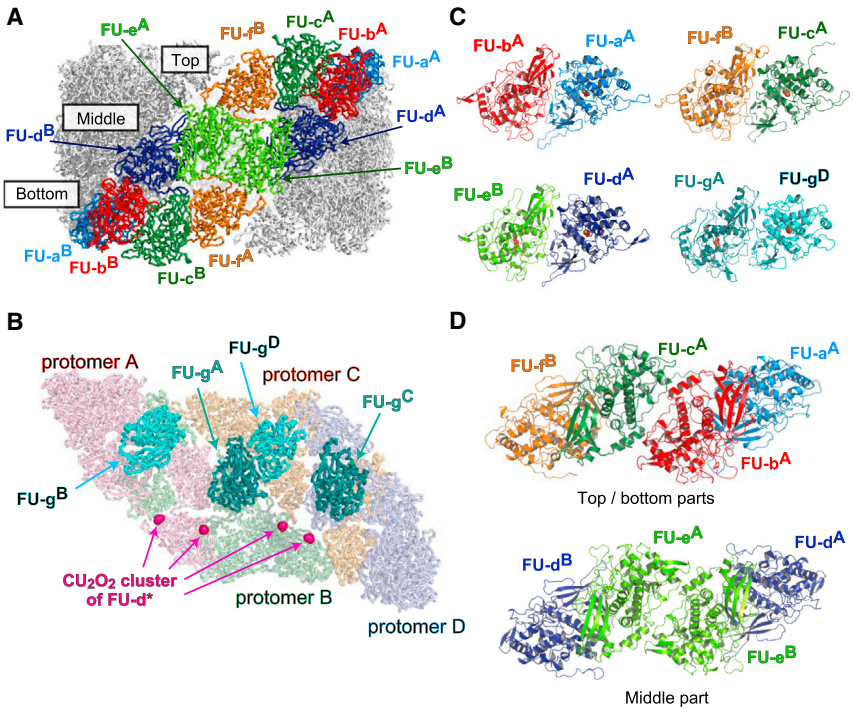

Figure 2. Structure of FU Dimer

(A) Location of FUs in the protomer-dimer. Each FU is colored according to Figure 1B.

(B) Structures of the collar region. Collar region between protomers A, B, C, and D viewed from inside the cylinder.

(C) Four types of FU dimers.

(D) Structure of the top/bottom parts and middle part of the wall region. Colors correspond to (A).

See also Tables S1, S2, and S3.

superposed on one another with RMSD < 2.1 Å. These observations indicate that the symmetrically located FU dimers act as building blocks to form the wall region. As observed for the wall FUs, FU-g of the inner collar region additionally forms a quite similar interprotomer FU dimer (e.g., FU-(g^A-g^D)) (Figures 2B and 2C). To stably assemble two plate-like protomer-dimers, an interprotomer FU-g dimer would be formed between two protomers. These FU arrangements coincide well with previous cryoelectron microscopic structures of other molluscan hemocyanins. Considered together, the entire cylindrical hemocyanin was constructed from FU dimer building blocks. The buried surface area within the FU dimer is significantly larger compared with other inter-FU interactions (Table S3), which additionally suggests the importance of FU dimer formation.

As described earlier, a warped plate-like dimer of protomers A and B acts as a structural unit in the five-fold symmetrical assembly (Figures 1A and 2A). The parallelogram wall of the protomer-dimer is divided into three parts: the top, middle, and bottom regions (Figure 2A). The middle region is composed of a pair of FU-(d^A-e^B). In contrast, the top and bottom regions are composed of two different FU dimers, FU-(a^A-b^A) and FU-(c^A-f^B). The relative orientation of the four FUs in the middle region (hereafter referred to as [FU-(d^B-e^A)] [FU-(e^B-d^A)]) is quite similar to those in the top and bottom regions ([FU-(a^A-b^A)][FU-(c^A-f^B)]) (Figure 2D). These observations indicate that the dimer of FU dimers (e.g., [FU-(d^B-e^A)] [FU-(e^B-d^A)]) is a unit forming the parallelogram wall of the protomer-dimer, in which three units are stacked.

Considered together, the architecture of the cylindrical hemocyanin is described as follows (Figure 3). First, two FUs assemble into an FU dimer with two-fold symmetry (step 1). Following this, two copies of the FU dimer further assemble to form a dimer of the FU dimer (e.g., [FU-(d^B-e^A)] [FU-(e^B-d^A)]) (step 2). The parallelogram wall region of the protomer-dimer is constructed by stacking three copies of this dimer of FU dimers (step 3). Five copies of the wall assemble into the cylindrical decamer with five-fold symmetry (step 4), stabilized by the interprotomer FU-g dimers of the collar region (Figure 3).

Interactions between FUs

In one protomer, an average of 91 inter-FU interactions (78 hydrogen bonds and 13 ion pairs) was found. Assuming that the interactions important for the assembly must be present in all ten equivalent interfaces, these interactions were analyzed. Table 2 shows the interactions conserved in all ten equivalent interfaces, which were quite few (i.e., only 12 hydrogen bonds and four ion pairs); furthermore, almost all were located at the interface within the FU dimer. Moreover, the conserved interactions were localized to two regions in the inter-FU interface (Figure 4). It should be noted that these two sites are related by the pseudo-two-fold symmetry between FUs. In addition to these specific interactions, the buried surface area within the FU dimer is significantly larger than other inter-FU interactions (Table S3). These observations indicate that the FU dimer is formed tightly through specific local interactions in combination with shape complementarity with a wide contact area.

Conversely, only three hydrogen bonds and a solo ion pair were conserved in the inter-FU dimer interactions (Table 2). These observations suggest that FU dimers interact with one another with substantial flexibility and few specific interactions. The relative orientation of the rigid FU dimers would be adjusted by less specific interactions between FU dimers, depending on their location, which might have allosteric effects on oxygen binding.

Many of the conserved specific interactions (i.e., 5 of 12 hydrogen bonds and 3 of 4 ion pairs) were formed between FU-a and -b (Table 2). In addition, the buried surface area of FU-(a-b) is the largest of the FU dimers (Table S3). These observations indicate that FU-a and -b intentionally form a tightly associated FU dimer. In contrast, the total buried surface area of FU-a is markedly smaller compared with other FUs, particularly in contacts other than FU dimer formation (Table S3), suggesting that FU-a forms fewer contacts with its neighboring FUs. To sustain rigidity as a building block, FU-a might need to be fixed on its counterpart much more tightly than other FUs.

Structure of FUs

All seven FUs had similar structures composed of two domains: the N-terminal core domain (NTD) and the C-terminal

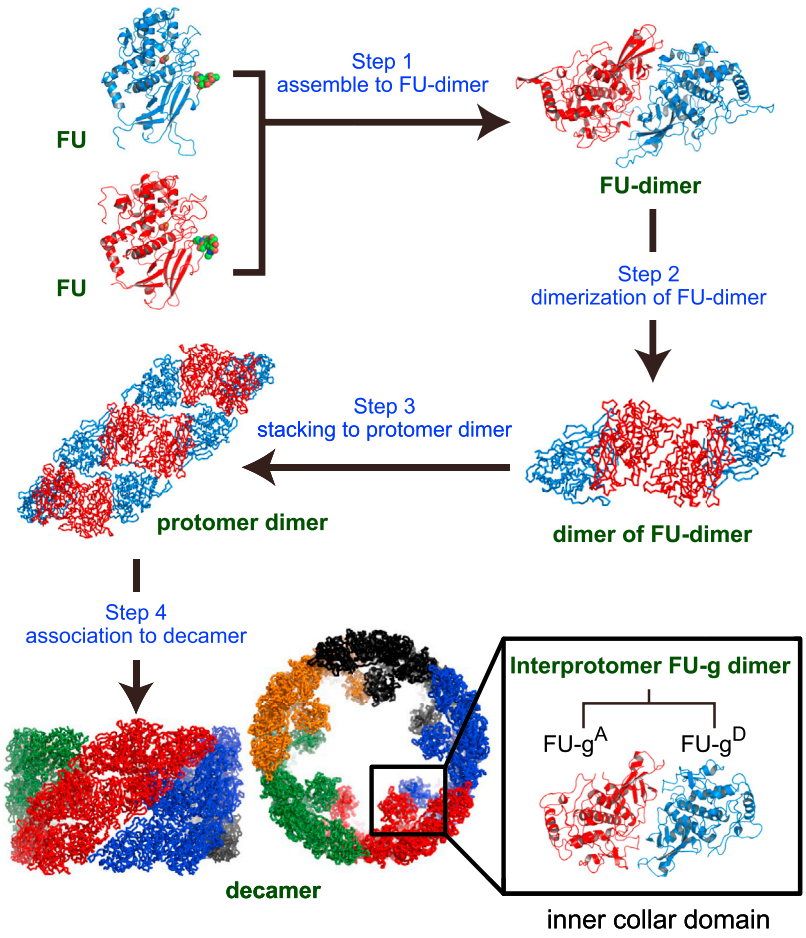

Figure 3. Architecture of Decameric Hemocyanin
(Step 1) Two FUs assemble into an FU dimer. (Step 2) Two FU dimers assemble into the dimer of the FU dimer. (Step 3) Three FU dimers corresponding to top, middle, and bottom regions stack on top of each other, resulting in the formation of a parallelogram protomer-dimer. (Step 4) Five protomer-dimers assemble with five-fold symmetry into a decamer, wherein protomer-dimers are stapled by the interprotomer FU-g dimer of the inner collar domain.

β-sandwich domain (CTD) (Figures 1C and 5A). The NTD was mainly composed of α helices, whereas the CTD was rich in β strands (Figures 5A and S2B). The anomalous difference Fourier map showed that all FUs contained two copper atoms (Cu1 and Cu2) at identical sites within their NTDs (Figures 1D, 5A, and S1E). Two oxygen atoms were bound between Cu1 and Cu2 to form a Cu_2O_2 cluster (Figures 5B and S4), in agreement with crystal absorption observed around 345 nm (Matsuno et al., 2015). The copper ions were coordinated by six His residues completely conserved among FUs: Cu1 coordinated with His41, His60, and His69, and Cu2 coordinated with His179, His183, and His210 (residue numbers correspond to FU-a). His60 formed a thioether bridge between the Cε atom and a sulfur atom of Cys58. In addition to these copper-coordinating residues, almost all other residues surrounding the site were common to all FUs. The geometry of the Cu_2O_2-binding site was quite similar in all FUs (Figure S4). Although the structure of hemocyanin was discussed based on the FU structures constructed by homology modeling hitherto, the atomic structure of the entire molecule determined in the present study made available the practical atomic structure of all FU types, and enables us to precisely discuss the hemocyanin structure based on the real structure, which is one of the important outcomes of this study.

The FUs share high structural similarity with pro-tyrosinase (Fujieda et al., 2013), a type-3 copper enzyme precursor (Figure S5): because of the common structural characteristics, these two proteins are considered to be derived from a common origin (Decker and Terwilliger, 2000). The NTDs and CTDs of hemocyanin FU correspond to the N-terminal catalytic and C-terminal shielding domains, respectively, of pro-tyrosinase. Although each domain was superposed onto its counterpart (RMSD 2.2 and 4.4 Å for NTD and CTD, respectively), the relative orientation between the two domains was shifted by approximately 17° (Figure S5). The structure surrounding the Cu_2O_2 cluster (i.e., coordination of six His residues and a thioether bridge between His and Cys) was well conserved. Furthermore, Phe65, Trp68, Glu176, Asn180, Phe206, and His209 were completely conserved in hemocyanin, commonly surrounding the directly coordinating His residues in pro-tyrosinase (Figures 5B, S5D, and S5E). These structural similarities between the two different proteins possessing similar copper clusters indicate that the surrounding environment as well as the direct coordination is important for maintaining the copper cluster stably.

All hemocyanin FUs formed FU dimers, a building block of hemocyanin, as described earlier (Figure 2). Although pro-tyrosinase also forms dimers (Fujieda et al., 2013), their manner of association is completely different. The FU dimer of hemocyanin is mainly formed through the CTD, whereas pro-tyrosinase dimers interact through the N-terminal catalytic domain (Figures S5F and S5G). In the pro-form of tyrosinase, the C-terminal shielding domain plays several important roles in maturation. This domain assists with copper incorporation into the active site using two Cys residues (Cys522 and Cys525), and the proteolytic cleavage of this domain activates pro-tyrosinase (Fujieda et al., 2013). Hemocyanin does not have these important Cys residues in its CTD despite the presence of a Cu_2O_2 cluster at the same site. In both proteins, the NTD acts as the functional domain while the CTD plays distinct roles (i.e., FU dimer formation in hemocyanin versus enzymatic maturation of tyrosinase). During evolution, each protein likely evolved the CTD according to its own requirement. Instead of the Cys residues necessary for copper incorporation, all FUs of hemocyanin have two other Cys residues (Cys47 and Cys57) in the vicinity of the Cu_2O_2 cluster, which form a disulfide bond (Figure 5C). These Cys residues are completely conserved among hemocyanins (Bergmann et al., 2006; Lieb et al., 2000; Miller et al., 1998; Stoeva et al., 1999, 2002; Thonig et al., 2014) while no tyrosinase possesses

Table 2. Inter-FU Interaction Completely Conserved among Ten Equivalent Interfaces

Atom 1			Atom 2			Averaged Distance (Å)	Location
Atom		FU	Atom		FU		
Hydrogen Bonds							
Lys 262	Nζ	a	Glu 795	Oε	b	2.55	Within FU dimer
Asp 374	O	a	Asn 661	Nδ	b	3.02	Within FU dimer
Val 401	O	a	Asn 661	N	b	2.92	Within FU dimer
Thr 402	Oγ	a	Cys 659	O	b	2.78	Within FU dimer
Tyr 403	N	a	Tyr 658	O	b	2.66	Within FU dimer
Lys 426	Nζ	b	Gly 1,123	O	c	2.91	Between FU dimers
Asn 1,071	O	c	Tyr 2,903	N	f	3.16	Within FU dimer
Ile 1,074	N	c	Leu 2,901	O	f	3.21	Within FU dimer
Asn 1,483	O	d	Arg 2,488	N	e	3.13	Within FU dimer
Phe 1,652	N	d	Asn 2,323	O	e	2.81	Within FU dimer
Gln 2,390	Nε	e	Gln 2,494	O	f	2.61	Between FU dimers
Gln 2,494	N	e	Ser 2,492	O	f	3.15	Between FU dimers
Ion Pairs							
Lys 262	Nζ	a	Glu 795	Oε	b	2.55	Within FU dimer
Arg 398	Nη	a	Glu 663	Oε	b	2.69	Within FU dimer
Arg 398	Nε	a	Glu 663	Oε	b	3.15	Within FU dimer
Glu 460	Oε	b	Arg 1,368	Nη	d	2.64	Between FU dimers

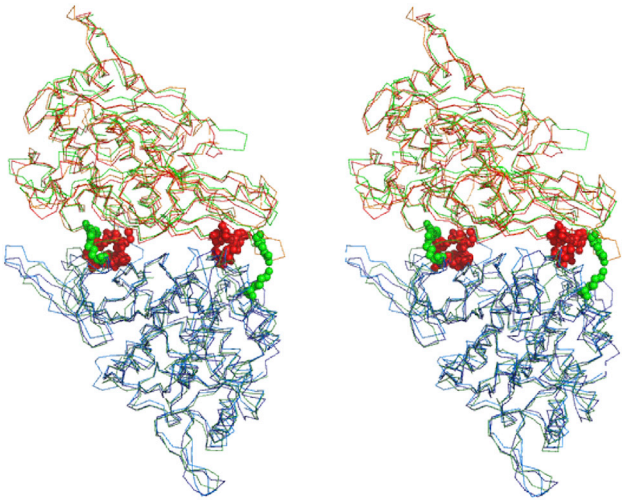

Figure 4. Location of Conserved Inter-FU interactions

(Stereo view) Residues forming hydrogen bonds and ion pairs conserved in all ten equivalent interfaces are shown as red and green spheres, respectively. For clarity, only inter-FU interactions within the FU dimer are shown. The colors of each ribbon diagram correspond to Figure 2A.

them (Fujieda et al., 2013). In addition, several highly conserved Met and Cys residues are located around them (Figure 5C). The caddie protein, a copper chaperone for tyrosinase, has been shown to use Met for copper relay (Matoba et al., 2011). These sulfur-containing residues surrounding the Cu_2O_2-binding site may play a role in copper transfer instead of Cys522 and Cys525 of the pro-tyrosinase C-terminal shielding domain.

Glycosylation

Hemocyanin is known to possess oligosaccharides. The structure revealed N-linked glycosylation at five of seven possible sites, including Asn387 of FU-a, Asn806 of FU-b, Asn1,498 and Asn1,636 of FU-d, and Asn2,472 of FU-e (Figures 1C and S2B). Four of these sites are located at identical positions within the CTD. In addition, FU-d possesses an additional glycan at Asn1,498 in the NTD. Chemical structure analysis of the oligosaccharides of *T. pacificus* hemocyanin revealed that the two most abundant sequences $(HexNAc)_1$ + $(Man)_3(GlcNac)_2$ and $(Hex)_1(HexNAc)_1$ + $(Man)_3(GlcNac)_2$ accounted for >95% of oligosaccharides in all individuals tested (Table S4). Both structures possessed a common root pentasaccharide structure; therefore, parts of $(Man)_3(GlcNac)_2$ were used for the observed electron density.

The oligosaccharides were all located on the outer surface of the wall and formed carbohydrate clusters (Figure 6A). The carbohydrates conjugated at Asn387 and Asn806 of protomer A (hereafter, glycan-387^A and glycan-806^A) formed a cluster with glycans-1,498^J, -1,636^J, and -2,472^I, which was located at the interface among three protomers, i.e., protomers A, I, and J. Furthermore, this site is located at the interface between two plate-like protomer-dimers. A cave is situated at the center of the cluster. These observations suggest that the carbohydrates reinforce the interaction through the wall regions between protomer-dimers. To evaluate the contribution of the carbohydrates to assembly, the effects of deglycosylation on reassociation of the hemocyanin subunit into the decamer were confirmed by electron microscopy (Figures 6B and S6A–S6C). Reassociation was significantly inhibited by treatment with glycosidase F, suggesting that carbohydrates play an important role in assembly. Furthermore, the addition of glucose caused a dramatic dissociation of hemocyanin (Figures 6C, S6D, and S6E). The interprotomer interaction by glycans would be competitively inhibited by the added sugars. These observations emphasize the significance of the glycans for the association of protomer-dimers. Although the inner collar stabilizes the interaction between adjacent protomer-dimers (Figure 2), its reinforcement using glycans might be necessary for stably maintaining the cylindrical decamer. Most of the glycan sites are conserved in other cephalopod hemocyanins (octopuses and cuttlefishes possess all five potential sites, whereas nautiluses possess four), whereas only two sites (glycan-387 and -1,498) are conserved in gastropod hemocyanins, suggesting that stabilization of assembly using glycans might be peculiar to cephalopod hemocyanins. Cephalopod hemocyanins generally do not possess FU-h, which contributes to the interprotomer interaction in gastropod hemocyanins. To compensate for the destabilization due to the loss of FU-h, cephalopod hemocyanins might be required to enhance the interprotomer interaction using glycans.

Zhang et al. (2013) reported previously that four FUs located at the interface between protomer-dimers, i.e., FU-a^A, -b^A, -d^J, and -e^I, form a "communication cluster" involved in the allosteric effect of hemocyanin. These FUs are proposed to act cooperatively in oxygen binding and release, in which interprotomer interactions by two long loops contribute significantly. In the crystal structure, these four FUs form a carbohydrate cluster, and furthermore, the two interacting loops are located in the

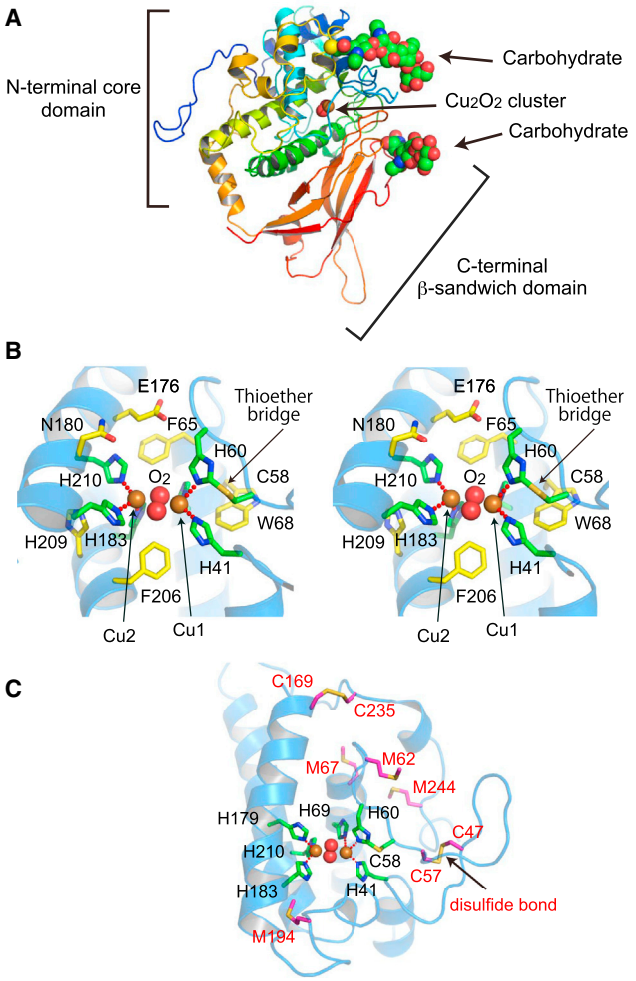

Figure 5. FU Structure

(A) Representative ribbon diagram of FU-d, colored as a ramp from blue (N terminus) to red (C terminus). The Cu_2O_2 cluster and carbohydrates are shown as spheres.

(B) Close-up view of the copper-binding site (stereo figure). His coordinating with coppers and Cys58 forming a thioether linkage to His60 are shown as green sticks. Residues conserved in both the hemocyanin FUs and prototyrosinase are shown as yellow sticks.

(C) Highly conserved sulfur-containing residues surrounding the Cu_2O_2-binding site (pink sticks).

See also Figures S2, S4, and S5.

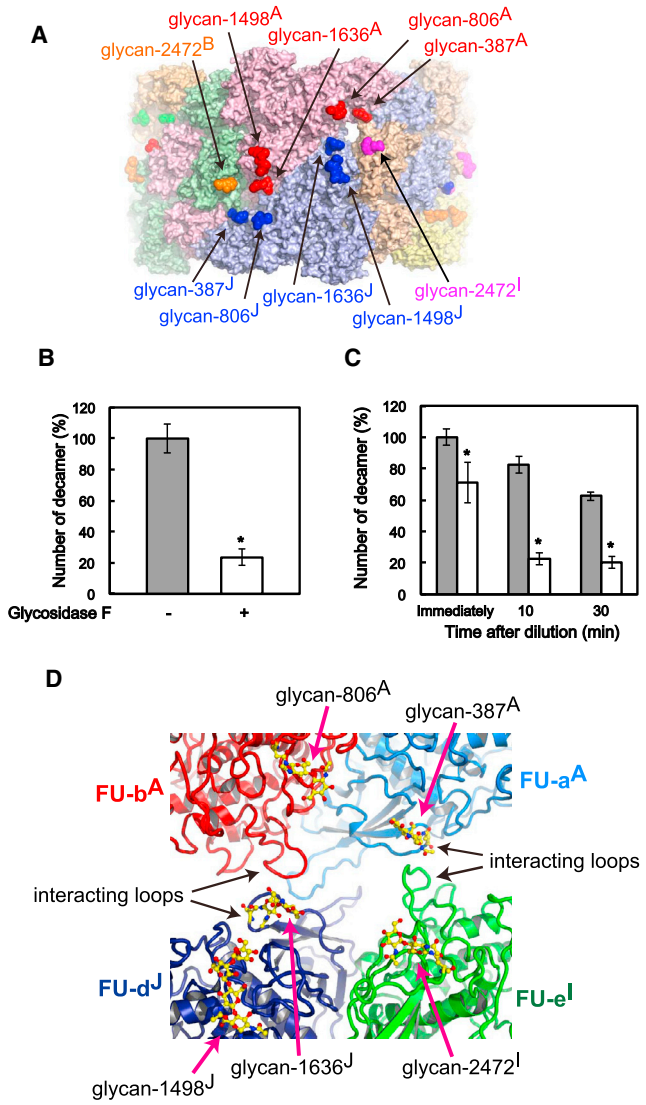

Figure 6. Carbohydrates and Their Effect

(A) Glycans on the hemocyanin decamer. Carbohydrates are shown as spheres.

(B) Effect of glycosidase treatment on decamer reassociation. Reassociation efficiency of dissociated hemocyanin subunits treated or untreated with glycosidase F was compared. The number of untreated hemocyanins was set to 100%. The error bars represent SD. *$p < 0.01$, Student's t test.

(C) Time dependency of the number of decamers in the absence (gray bars) or presence (white bars) of glucose. The error bars represent SD. *$p < 0.01$, Student's t test.

(D) Close-up view of the carbohydrate cluster. Carbohydrates are shown as balls and sticks. Loops interacting between FUs are indicated by a black arrow.

See also Figures S2 and S6, and Table S4.

vicinity of the cluster. Moreover, glycan-387^A and -1,636^J are located on one of the loops (Figure 6D). Importantly, N-linked glycan sites for these two glycans are completely conserved in all known hemocyanins. These observations strongly indicate the contribution of these two conserved glycans to the allosteric effect as well as reinforcing interprotomer interaction.

Although the carbohydrates on hemocyanin have been extensively studied, neither their precise location nor their function had been elucidated completely. The present study resolved these uncertainties. The atomic coordinates will enable the design of hemocyanin. We hope that our crystal structure of intact hemocyanin will facilitate future developments in both bioengineering and fundamental scientific research.

EXPERIMENTAL PROCEDURES

Structure Analysis

The procedures of crystallization and X-ray data collection have been previously described (Matsuno et al., 2015). The initial phase was determined at 10 Å resolution by molecular replacement using the PHASER program (McCoy et al., 2007) with the Cα model of the wall region of *H. diversicolor* hemocyanin determined by cryoelectron microscopy (PDB: 3J32) (Zhang et al., 2013) as a

search model. The phase was improved by NCS averaging using DM from the CCP4 program package (Collaborative Computational Project Number 4, 1994). Model building was manually performed using Coot (Emsley et al., 2010). Parts of $(Man)_3(GlcNac)_2$ were used for the electron density of oligosaccharides because the chemical structure analysis of the oligosaccharides of *T. pacificus* hemocyanin revealed that >95% of the glycans commonly had $(Man)_3(GlcNac)_2$ as a root structure. Structure refinement was performed using phenix.refine (Adams et al., 2010). Atoms in the wall region were refined individually, whereas rigid body refinement in combination with group adp refinement were applied to the FU-g because of the ambiguous electron density owing to overlap and flexibility of this FU. The structure of FU-g used as rigid body was constructed based on the NCS averaged map, applying D_5 symmetry. Since alternative conformers of FU-g are derived from intermingling of two opposite orientations, an occupancy of 0.5 was assigned to all FU-g. For FU-d*, only the Cu_2O_2 cluster was located, because the anomalous difference Fourier map clearly showed the sites of Cu_2O_2 cluster, although overall structure of FU-d* was not constructed owing to overlap of electron density. Since the pathway was not determined due to the poor electron density of the linker between wall and collar regions, the fragment of FU-a–d, FU-e–f, and FU-g were assigned as different chains.

To monitor refinement, a random 5% subset of all reflections was set aside for calculation of the R_{free} value. R_{work} and R_{free} values finally converged to 27.4% and 30.3%, respectively. The stereochemical quality of the refined structure was calculated by MolProbity (Chen et al., 2010) as follows: the Ramachandran plot favored 94.3%, allowed 4.97%, with 0.73% outliers. The buried surface area and number of hydrogen bonds and ion pairs were calculated using CONTACT from the CCP4 program package (Collaborative Computational Project Number 4, 1994). The *Z* score and RMSD were calculated using combinatorial extension (Shindyalov and Bourne, 1998). The anomalous difference Fourier map was calculated using PHASER (McCoy et al., 2007) from diffraction data at 5.15 Å resolution collected at the absorption edge of copper (1.3781 Å) at beamline BL17A of the Photon Factory. Crystallographic data and refinement statistics are summarized in Table 1 The atomic coordinates have been deposited in the PDB, www.pdb.org (PDB: 4YD9).

Determination of Amino Acid Sequence

The amino acid sequence was determined from genomic DNA isolated from testis of *T. pacificus* using ISOHAIR (Nippon Gene). Gene fragments of hemocyanin were PCR amplified from isolated genomic DNA using synthesized primers, and cloned into a pGEM-T easy vector (Promega). The sequences of the cloned fragments were confirmed by 3130 Genetic Analyzer (Life Technologies). The exon region was determined using GENSCAN 1.0 (Burge and Karlin, 1997) and SPLICEPORT (Dogan et al., 2007) programs using the previously determined sequence of *Sepia officinalis* (Thonig et al., 2014) as a reference. The 18,399-bp-long genomic sequence and 3,314-residue amino acid sequence were deposited in DDBJ/EMBL/GenBank (DDBJ: AB897790).

Carbohydrate Analysis

N-Linked oligosaccharides were analyzed using a glycoblotting-based method, as described previously (Nishimura et al., 2004). Purified hemocyanin (0.1 mg) was reduced and alkylated in the presence of a detergent and then digested by trypsin. N-Glycans of glycopeptides were released from trypsin-digested samples by incubation with N-glycosidase F (New England Biolabs) or N-glycosidase A (Roche Applied Science) and then specifically captured on BlotGlyco H beads via hydrazone bonds. The glycans blotted on beads were purified using the Mass PREP HILIC μElution Plate (Waters) and subjected to MALDI-TOF mass spectrometry (MS) analysis using an Ultraflex time-of-flight mass spectrometer III (Bruker Daltonics) in reflector positive ion mode with 2,5-dihydroxylbenzoic acid as a matrix. The detected N-glycan peaks in MALDI-TOF MS spectra were chosen using FlexAnalysis v. 3 software (Bruker Daltonics). The intensity of the isotopic peaks of each glycan was normalized to a 10-pmol internal standard (A2 amide glycan). Glycan structures were determined using the GlycoMod Tool (http://web.expasy.org/glycomod/) and the GlycoSuite website (http://unicarbkb.org/).

Electron Microscopy

Specimens for electron microscopy were negatively stained with 1% (w/v) uranyl acetate and examined under a Hitachi H-7650 transmission electron microscope (Hitachi High-Technologies) at an accelerating voltage of 80 kV and 20,000× magnification.

Glycosidase Treatment

The hemocyanin subunit (560 μg) was treated with 1,000 U of N-glycosidase F for 24 hr at 20°C, followed by 24 hr incubation at 4°C. The subunit was also prepared without glycosidase treatment as a negative control. The absence or presence of the N-glycans was confirmed by periodic acid-Schiff staining. To reassociate the decamer, glycosidase-treated or -untreated subunits (3 mg/ml) were dialyzed against reassociation buffer containing 150 mM $CaCl_2$ and 100 mM HEPES (pH 7.5) overnight at 4°C. Reassociation was confirmed by electron microscopy. Specimens for electron microscopy were immediately prepared after 100× dilution with reassociation buffer. Ten images were taken from each specimen and the number of decamers on each image counted. The mean number of decamers was compared, and the negative control was set as 100%. Results are presented as the mean ± SEM.

Effect of Glucose on Decameric Structure

Hemolymph was diluted with a solution containing 0.5 M NaCl and 10 mM HEPES (pH 7.0) with or without 10 mM glucose to produce a hemocyanin concentration of 20 μg/ml. Specimens for electron microscopy were prepared after incubating for the desired period after dilution. Thirty images were taken from each specimen, and the number of decamers on each image was counted. The mean number of decamers in the solution without glucose immediately after dilution was set as 100%. Results are presented as the mean ± SEM.

ACCESSION NUMBERS

The accession number for the crystal structure reported in this paper is PDB: 4YD9. The accession number for the sequence reported in this paper is DDBJ: AB897790.

SUPPLEMENTAL INFORMATION

Supplemental Information includes six figures, four tables, and conf1-all.pdb and can be found with this article online at http://dx.doi.org/10.1016/j.str.2015.09.008.

AUTHOR CONTRIBUTIONS

Y.T., M.Y., S.K., T.S., and H.K. designed research. Z.G., A.M., and K.K. determined crystal structure. S.K. and M.R.I.K. performed electron microscopic analysis. T.S., T.Y., Y.K., H.K., G.K., and Y.M. determined sequence. T.T. and Y.T. analyzed the data.

ACKNOWLEDGMENTS

We thank Prof. Isao Tanaka of Hokkaido University (Japan) for his helpful discussions. This work was supported by JSPS KAKENHI, grant numbers 26291008, 24000011, 26102501 (to Y.T.) and 25450298 (to S.K.), Platform for Drug Discovery, Informatics, and Structural Life Science (to S.K. and Y.T.), and Regional Innovation Strategy Support Program (to S.K., T.S., T.Y., and Y.K.) from the Ministry of Education, Culture, Sports, Science and Technology (Japan). The X-ray diffraction experiments were performed under the proposal numbers 2013G165, 2015G067 (Photon Factory), 2013A6829, 2013A1096, 2013B6829, 2013B1031, 2014A1193, 2014B6930, 2014B1295, 2014B1292, 2015A6524, 2015A1114 (SPring-8), and 20121296 (Swiss Light Source).

Received: April 16, 2015
Revised: September 3, 2015
Accepted: September 14, 2015
Published: October 22, 2015

REFERENCES

Adams, P.D., Afonine, P.V., Bunkoczi, G., Chen, V.B., Davis, I.W., Echols, N., Headd, J.J., Hung, L.W., Kapral, G.J., Grosse-Kunstleve, R.W., et al. (2010).

PHENIX: a comprehensive Python-based system for macromolecular structure solution. Acta Crystallogr. D Biol. Crystallogr. *66*, 213–221.

Becker, M.I., Arancibia, S., Salazar, F., Campo, M.D., and Ioannes, A.D. (2014). Mollusk hemocyanins as natural immunostimulants in biomedical applications. In Immune Response Activation, G.H.T. Duc, ed. (InTech), pp. 45–72.

Bergmann, S., Lieb, B., Ruth, P., and Markl, J. (2006). The hemocyanin from a living fossil, the cephalopod *Nautilus pompilius*: protein structure, gene organization, and evolution. J. Mol. Evol. *62*, 362–374.

Boisset, N., and Mouche, F. (2000). *Sepia officinalis* hemocyanin: a refined 3D structure from field emission gun cryoelectron microscopy. J. Mol. Biol. *296*, 459–472.

Burge, C., and Karlin, S. (1997). Prediction of complete gene structures in human genomic DNA. J. Mol. Biol. *268*, 78–94.

Chen, V.B., Arendall, W.B., 3rd, Headd, J.J., Keedy, D.A., Immormino, R.M., Kapral, G.J., Murray, L.W., Richardson, J.S., and Richardson, D.C. (2010). MolProbity: all-atom structure validation for macromolecular crystallography. Acta crystallographica. Section D. Biol. Crystallogr. *66*, 12–21.

Collaborative Computational Project Number 4. (1994). The CCP4 suite: programs for protein crystallography. Acta Crystallogr. D Biol. Crystallogr. *50*, 760–763.

Cuff, M.E., Miller, K.I., van Holde, K.E., and Hendrickson, W.A. (1998). Crystal structure of a functional unit from octopus hemocyanin. J. Mol. Biol. *278*, 855–870.

Decker, H., and Terwilliger, N. (2000). Cops and robbers: putative evolution of copper oxygen-binding proteins. J. Exp. Biol. *203*, 1777–1782.

Dogan, R.I., Getoor, L., Wilbur, W.J., and Mount, S.M. (2007). SplicePort—an interactive splice-site analysis tool. Nucleic Acids Res. *35*, W285–W291.

Emsley, P., Lohkamp, B., Scott, W.G., and Cowtan, K. (2010). Features and development of Coot. Acta Crystallogr. D Biol. Crystallogr. *66*, 486–501.

Fujieda, N., Yabuta, S., Ikeda, T., Oyama, T., Muraki, N., Kurisu, G., and Itoh, S. (2013). Crystal structures of copper-depleted and copper-bound fungal pro-tyrosinase: insights into endogenous cysteine-dependent copper incorporation. J. Biol. Chem. *288*, 22128–22140.

Gatsogiannis, C., and Markl, J. (2009). Keyhole limpet hemocyanin: 9-A CryoEM structure and molecular model of the KLH1 didecamer reveal the interfaces and intricate topology of the 160 functional units. J. Mol. Biol. *385*, 963–983.

Gatsogiannis, C., Moeller, A., Depoix, F., Meissner, U., and Markl, J. (2007). *Nautilus pompilius* hemocyanin: 9 A cryo-EM structure and molecular model reveal the subunit pathway and the interfaces between the 70 functional units. J. Mol. Biol. *374*, 465–486.

Gatsogiannis, C., Hofnagel, O., Markl, J., and Raunser, S. (2015). Structure of mega-hemocyanin reveals protein origami in snails. Structure *23*, 93–103.

Geyer, H., Wuhrer, M., Resemann, A., and Geyer, R. (2005). Identification and characterization of keyhole limpet hemocyanin N-glycans mediating cross-reactivity with *Schistosoma mansoni*. J. Biol. Chem. *280*, 40731–40748.

Harris, J.R., and Markl, J. (1999). Keyhole limpet hemocyanin (KLH): a biomedical review. Micron *30*, 597–623.

Harris, J.R., Meissner, U., Gebauer, W., and Markl, J. (2004). 3D reconstruction of the hemocyanin subunit dimer from the chiton *Acanthochiton fascicularis*. Micron *35*, 23–26.

Jaenicke, E., Buchler, K., Markl, J., Decker, H., and Barends, T.R. (2010). Cupredoxin-like domains in haemocyanins. Biochem. J. *426*, 373–378.

Jaenicke, E., Buchler, K., Decker, H., Markl, J., and Schroder, G.F. (2011). The refined structure of functional unit h of keyhole limpet hemocyanin (KLH1-h) reveals disulfide bridges. IUBMB Life *63*, 183–187.

Lamy, J., You, V., Taveau, J.C., Boisset, N., and Lamy, J.N. (1998). Intramolecular localization of the functional units of *Sepia officinalis* hemocyanin by immunoelectron microscopy. J. Mol. Biol. *284*, 1051–1074.

Lieb, B., Altenhein, B., and Markl, J. (2000). The sequence of a gastropod hemocyanin (HtH1 from Haliotis tuberculata). J. Biol. Chem. *275*, 5675–5681.

Markl, J. (2013). Evolution of molluscan hemocyanin structures. Biochim. Biophys. Acta *1834*, 1840–1852.

Matoba, Y., Bando, N., Oda, K., Noda, M., Higashikawa, F., Kumagai, T., and Sugiyama, M. (2011). A molecular mechanism for copper transportation to tyrosinase that is assisted by a metallochaperone, caddie protein. J. Biol. Chem. *286*, 30219–30231.

Matsuno, A., Gai, Z., Tanaka, M., Kato, K., Kato, S., Katoh, T., Shimizu, T., Yoshioka, T., Kishimura, H., Tanaka, Y., et al. (2015). Crystallization and preliminary X-ray crystallographic study of a 3.8-MDa respiratory supermolecule hemocyanin. J. Struct. Biol. *190*, 379–382.

McCoy, A.J., Grosse-Kunstleve, R.W., Adams, P.D., Winn, M.D., Storoni, L.C., and Read, R.J. (2007). Phaser crystallographic software. J. Appl. Crystallogr. *40*, 658–674.

Meissner, U., Dube, P., Harris, J.R., Stark, H., and Markl, J. (2000). Structure of a molluscan hemocyanin didecamer (HtH1 from *Haliotis tuberculata*) at 12 A resolution by cryoelectron microscopy. J. Mol. Biol. *298*, 21–34.

Miller, K.I., Schabtach, E., and van Holde, K.E. (1990). Arrangement of subunits and domains within the *Octopus dofleini* hemocyanin molecule. Proc. Natl. Acad. Sci. USA *87*, 1496–1500.

Miller, K.I., Cuff, M.E., Lang, W.F., Varga-Weisz, P., Field, K.G., and van Holde, K.E. (1998). Sequence of the *Octopus dofleini* hemocyanin subunit: structural and evolutionary implications. J. Mol. Biol. *278*, 827–842.

Nishimura, S., Niikura, K., Kurogochi, M., Matsushita, T., Fumoto, M., Hinou, H., Kamitani, R., Nakagawa, H., Deguchi, K., Miura, N., et al. (2004). High-throughput protein glycomics: combined use of chemoselective glycoblotting and MALDI-TOF/TOF mass spectrometry. Angew. Chem. Int. Ed. Engl. *44*, 91–96.

Perbandt, M., Guthohrlein, E.W., Rypniewski, W., Idakieva, K., Stoeva, S., Voelter, W., Genov, N., and Betzel, C. (2003). The structure of a functional unit from the wall of a gastropod hemocyanin offers a possible mechanism for cooperativity. Biochemistry *42*, 6341–6346.

Shindyalov, I.N., and Bourne, P.E. (1998). Protein structure alignment by incremental combinatorial extension (CE) of the optimal path. Protein Eng. *11*, 739–747.

Siddiqui, N.I., Idakieva, K., Demarsin, B., Doumanova, L., Compernolle, F., and Gielens, C. (2007). Involvement of glycan chains in the antigenicity of *Rapana thomasiana* hemocyanin. Biochem. Biophys. Res. Commun. *361*, 705–711.

Stoeva, S., Schutz, J., Gebauer, W., Hundsdorfer, T., Manz, C., Markl, J., and Voelter, W. (1999). Primary structure and unusual carbohydrate moiety of functional unit 2-c of keyhole limpet hemocyanin (KLH). Biochim. Biophys. Acta *1435*, 94–109.

Stoeva, S., Idakieva, K., Betzel, C., Genov, N., and Voelter, W. (2002). Amino acid sequence and glycosylation of functional unit RtH2-e from *Rapana thomasiana* (gastropod) hemocyanin. Arch. Biochem. Biophys. *399*, 149–158.

Thonig, A., Oellermann, M., Lieb, B., and Mark, F.C. (2014). A new haemocyanin in cuttlefish (*Sepia officinalis*) eggs: sequence analysis and relevance during ontogeny. EvoDevo *5*, 6.

Zhang, Q., Dai, X., Cong, Y., Zhang, J., Chen, D.H., Dougherty, M.T., Wang, J., Ludtke, S.J., Schmid, M.F., and Chiu, W. (2013). Cryo-EM structure of a molluscan hemocyanin suggests its allosteric mechanism. Structure *21*, 604–613.

Zhu, H., Zhuang, J., Feng, H., Liang, R., Wang, J., Xie, L., and Zhu, P. (2014). Cryo-EM structure of isomeric molluscan hemocyanin triggered by viral infection. PLoS One *9*, e98766.

